Photoionization study of Kr+ and Xe+ ions with the combined use of a merged-beam set-up and an ion trap

J M Bizau, C Blancard, M Coreno, D Cubaynes, C Dehon, N El Hassan, F Folkmann, M F Gharaibeh, A Giuliani, J Lemaire, et al.

▶ **To cite this version:**

J M Bizau, C Blancard, M Coreno, D Cubaynes, C Dehon, et al.. Photoionization study of Kr+ and Xe+ ions with the combined use of a merged-beam set-up and an ion trap. Journal of Physics B: Atomic, Molecular and Optical Physics, 2011, 44 (5), pp.55205. 10.1088/0953-4075/44/5/055205 . hal-00630012

HAL Id: hal-00630012
https://hal.science/hal-00630012

Submitted on 7 Oct 2011

HAL is a multi-disciplinary open access archive for the deposit and dissemination of scientific research documents, whether they are published or not. The documents may come from teaching and research institutions in France or abroad, or from public or private research centers.

L'archive ouverte pluridisciplinaire **HAL**, est destinée au dépôt et à la diffusion de documents scientifiques de niveau recherche, publiés ou non, émanant des établissements d'enseignement et de recherche français ou étrangers, des laboratoires publics ou privés.

Photoionization study of Kr^+ and Xe^+ ions with the combined use of a merged-beam set-up and an ion trap.

J M Bizau[1], C Blancard[2], M Coreno[3], D Cubaynes[1], C Dehon[4], N El Hassan[1], F Folkmann[5], M F Gharaibeh[6], A Giuliani[7,8], J Lemaire[4], A R Milosavljević[8,9] C Nicolas[8] and R Thissen[10]

[1] Institut des Sciences Moléculaires d'Orsay (ISMO), CNRS UMR 8214, Université Paris-Sud, Bât. 350, F-91405 Orsay cedex, France
[2] CEA-DAM-DIF, Bruyères-le-Châtel, F-91297 Arpajon Cedex, France
[3] CNR—IMIP, Rome branch and Gas Phase Beamline@Elettra, I-34012 Trieste, Italy
[4] Laboratoire de Chimie Physique, CNRS UMR 8000, Université Paris Sud, Bât 350, F-91405 Orsay, France
[5] Department of Physics and Astronomy, University of Aarhus, DK-8000 Aarhus C, Denmark
[6] Jordan University of Sciences and Technology, Irbid 22110, Jordan
[7] Cepia, Institut National de la Recherche Agronomique (INRA), BP 71627, F-44316 Nantes Cedex 3, France
[8] Synchrotron SOLEIL, L'Orme des Merisiers, Saint Aubin, BP 48, F-91192 Gif-sur-Yvette cedex, France
[9] Institute of Physics, University of Belgrade, Pregrevica118, 11080 Belgrade, Serbia
[10] UJF-Grenoble 1 / CNRS-INSU, Institut de Planétologie et d'Astrophysique de Grenoble (IPAG) UMR 5274, Grenoble, F-38041, France

E-mail: jean-marc.bizau@u-psud.fr

Abstract. Photoionization cross sections of halogen-like Kr^+ and Xe^+ ions have been measured in the photon energy range extending up to 15 eV above the threshold. Two different devices were used, a merged-beam set-up and an ion trap. Combination of the two techniques allows the extraction of the pure ground state ionization cross section on an absolute scale. MCDF calculations reproduce well the magnitude of the direct photoionization cross sections.

PACS numbers: 32.80.Fb, 32.80.Zb

1. Introduction:

Atomic physics provides unique tools for plasma diagnostics. In particular, based on photoionization studies on ionic species one can deduce essential spectroscopic data for the determination of important plasma parameters such as abundance and temperature. In addition, dipole selection rules allow further simplification of the data by reducing the number of allowed transitions. To be useful, quantities like the energies and oscillator strengths of discrete lines or direct photoionization cross sections must be measured in absolute value with high accuracy for a large number of ionic species and over a wide range of photon energy. Photoionization is also one of the main processes contributing to plasma opacity and radiation transfer inside plasmas.

Krypton and xenon ions are of particular importance in tokamak plasmas. Injection of high-Z gases, essentially Kr and Xe, has been proposed as a technique to mitigate disruption [1,2], i.e. the uncontrolled and sudden loss of tokamak plasma current and energy. Disruption can produce severe damage on the vessel wall. The situation becomes more delicate for large machines such as ITER (International Thermonuclear Experimental Reactor), where incident loading energy may reach several GW/m^2 [3,4]. After injection of the gases, highly charged Kr and Xe ions are dominant in the core of the plasma, and low-charged and singly charged ions are abundant near the edge.

Experimentally, photoionization data on ionic targets have been obtained using mainly two techniques: DLPP (Dual Laser Produced Plasma) and merged-beam in synchrotron radiation facilities. While the former technique measures photoabsorption spectra [5], the latter provides absolute single and multiple photoionization cross sections [6,7]. Up to now, only the K shell photoionization of the Kr^+ ion has been reported [8], and all studies on the Xe^+ ion have focused on the region of 4d subshell excitation and ionization using the merged beam technique [9-13]. To best of our knowledge, no studies using these techniques have been published on the Kr^+ ion or on the Xe^+ ion in another energy range and, in particular, close to the thresholds. On the top of that no theoretical results on the photoionization processes are available for these ions outside the region of 4d excitation in the Xe^+ ion.

One difficulty, suffered both by the DLPP and merged-beam techniques, relates to the composition of the ionic target. Very often, it is made of a mixture of ions in the ground and metastable states, and most of the time in unknown relative proportion. Attempts have been achieved to determine experimentally the population of excited states inside the target. In DLPP experiments, this can be done, to a certain extent, by taking advantage of the time- and space-resolved capabilities of the technique which allows probing with the ionizing radiation regions of different temperatures in the plasma target, and enhancing the contribution of ions in the ground state or the metastable states [14]. In merged-beam experiments, the populations can be determined by measuring the attenuation of the ion beam passing through a gas cell, taking advantage of the different magnitude of the electron capture cross section for the ions in the ground state and the metastable states [15-18]. Another method, applied in the case of the Sc^{2+} ion, consisted of comparing, via the detailed balance principle, the intensity of the resonant photoionization cross section of Sc^{2+} with the previously measured dielectronic recombination cross section of Sc^{3+} [19,20]. This procedure was possible only because one channel strongly dominates the radiative decay of the recombination resonances in Sc^{2+}. Except for these few examples, in all other studies the relative populations were estimated by normalization to some theoretical results, or by assuming a statistical population when the mean electron kinetic energy in the plasma used to produce the ions is well above the energy needed to excite metastable states.

In 2008, we proposed an alternative method to avoid the problem introduced by the production of metastable states in the target: to use a trap to store the ions before irradiation during a time long enough to allow the excited states to radiatively decay to the ground state and, after irradiation *in situ*, to analyze the charge of the ions. The feasibility of the concept was demonstrated using a Fourier Transform Ion Cyclotron Resonance (FT-ICR) trap at the Gas Phase beam line of ELETTRA [21]. The photoionization spectrum of Xe^+ ion in the pure $5p^5\ ^2P_{3/2}$ ground state was measured in the 20-25 eV photon energy range. Before this experiment, only a few attempts to couple an ion trap with a beam of XUV light had been performed. Kravis *et al* [22,23] have obtained the charge distribution of the photoions formed by broadband irradiation with synchrotron light of Ar^{2+} ions stored in a Penning trap. More recently, Epp *et al* [24] have used the ultra-brilliant light from the Free Electron Laser (FEL) in Hamburg to demonstrate the feasibility of performing laser spectroscopy on Fe^{23+} ions produced in an Electron Beam Ion Trap (EBIT). Recently, the same EBIT was used at BESSY II to record photoionization spectra of some multiply-charged ions [25]. Hirsch *et al* [26] have also used a linear trap at BESSY II to measure photoionization spectra of mass selected clusters.

In this paper, we present our results on photoionization of Kr^+ and Xe^+ ions in the energy range covering 15 eV above the first ionization threshold, using both merged-beam and FT-ICR devices. With the merged beam set-up, the absolute photoionization cross sections for a mixture of ions in

the $np^5\ ^2P_{3/2}$ ground level (n = 4 for Kr and n = 5 for Xe) and $np^5\ ^2P_{1/2}$ metastable level have been determined. With the trap, the photoionization cross section for the ions in the pure $np^5\ ^2P_{3/2}$ ground level has been recorded in relative value. Combination of the two techniques allows the data obtained with the trap to be placed on an absolute scale. MCDF calculations have been performed to help in the interpretation of the data. In the following, after the description of the two devices and the experimental procedures, we will present and discuss the results. To conclude, future developments of the ion trap technique for photoionization studies on ionic species will be commented upon.

2. Experimental procedures

2.1. Merged-beam experiment

Measurements were performed using the ASTRID merged-beam set-up at the University of Aarhus in Denmark. The characteristics of the set-up and the experimental procedure used to extract absolute photoionization cross sections from the measurements have already been described in detail [27]. In short, the photons are supplied by synchrotron radiation from the 30-period undulator beam line at the ASTRID storage ring. Synchrotron radiation is monochromatized by a Miyake type monochromator [28] composed of one 1200 lines/mm plane grating covering the 15-180 eV photon energy range. In order to avoid higher-order radiation from being diffracted by the grating, a Mg filter is inserted at the exit of the monochromator. The photon flux is measured by an Al_2O_3 photodiode. Photodiode efficiency and photon energy are determined in real time using an ionization chamber of the double-collector type originally developed by Samson [29]. For energy calibration, $3s \rightarrow np$ excitation lines in argon and $2s \rightarrow np$ excitation lines in neon were used [30]. Accuracy on the photon energy scale is estimated to be 20 meV.

Kr^+ and Xe^+ target ions are produced using a hot-filament plasma ion source of the Nielsen type [31]. The ions are extracted from the ion source and accelerated using a 2 kV extraction voltage, mass separated by a dipole magnet, collimated and merged electrostatically with the photon beam. The interaction between photons and ions takes place in a ~50 cm long cylinder, biased to +600 V in order to obtain a well defined interaction length by energy marking of the photoions. To measure the profiles of the two beams and their mutual overlap, three sets of xy scanners are placed along this cylinder. Typical currents of 20 nA of target ions were obtained in the interaction region. The signal of photoions and the primary ion beam are separated by a second dipole magnet. The current of primary ion beam is measured in a Faraday cup. To reduce the background of scattered ions, the beam of photoions is further separated by an electrostatic analyser before the ions are detected by a particle detector similar to the one described by Rinn *et al* [32]. A chopper is inserted at the exit of the monochromator to measure the background signal on the detector produced by ions scattered by slits, ionization resulting from collisions between ions from the target beam and residual gas molecules, and highly-excited metastable ions that are emitted by the ion source and that decay in the interaction region by autoionization. Typical signal/noise ratio measured on the detector was 30 Hz/10 Hz at photon energy 10 eV above threshold.

The absolute photoionization cross sections σ are calculated from measurements of the current I of the target-ion beam, the photon beam intensity ($=J/e\eta$, from the photodiode current J with efficiency η), the ion and photon beam profiles, the velocity v and charge stage q of the target ions, the photoion counting rate S, the efficiency of the particle detector Ω, and the length of the interaction region L as follows:

$$\sigma = \frac{Se^2\eta vq}{IJ\Omega\int_0^L \frac{dz}{\Delta x \Delta y F(z)}} \qquad (1)$$

$\Delta x \Delta y F(z)$ is an effective beam area (z is the propagation axis of the two beams), and F is a two dimensional form factor defined by

$$F_{xy} \approx \frac{\sum i_{xy} \sum j_{xy}}{\sum \sum i_{xy} j_{xy}} \quad (2)$$

where $i_{xy} = i(x,y)\Delta x \Delta y$ and $j_{xy} = j(x,y)\ \Delta x \Delta y$ are the ion and photon currents, respectively, recorded during the beam-profile measurements and Δx and Δy the step sizes involved in these scans, typically 0.2 mm.

Accuracy of the cross-section data was determined by statistical fluctuations and the systematic contributions resulting from the measurement of the different parameters in equation (1). Above 25 eV photon energy, the latter is estimated to be 15% and is dominated by the uncertainty in the determination of the absolute photon flux, in particular due to the possible contribution of high-order radiation, and the determination of the detector efficiency [27]. Below 25 eV, the magnitude of photoionization cross sections might be underestimated and the systematic uncertainties cannot be estimated, since second order radiation is not filtered out by the Mg filter and contributes in an unknown proportion to the measured photon flux.

2.2. FT-ICR ion trap

In the present experiment, we have used the FT-ICR ion trap already used at ELETTRA [21]. The concept of coupling a FT-ICR to a light source has been already applied with great success to perform spectroscopy of selectively prepared ions by Infra-Red Multi-Photon Dissociation (IRMPD) on Infra-Red FEL [33,34]. The MICRA (Mobile Ion Cyclotron Resonance Analyzer) spectrometer, the same used at the CLIO Infra-Red FEL in Orsay, France and the Gas Phase beam line at ELETTRA, Italy, has been installed on branch B of the DESIRS beam line of the storage ring SOLEIL, Saint Aubin in France. The synchrotron radiation, produced in a 15-period electromagnetic undulator, is monochromatized by a normal incidence monochromator delivering photons in the 5-40 eV energy range. A new 400 lines/mm low dispersion grating and 700 μm exit slit width were used to obtain high flux, resulting in a bandpass of 100 meV. Optics cut-off produced by the normal incidence of the light on the grating provides spectral purity above 21 eV photon energy.

The FT-ICR traps are based on a strong magnetic field, trapping the ions in two dimensions, and an electrostatic field creating a potential well in the third dimension. The particularity of FT-ICR traps is that the ions can be excited *in-situ* and create an image current on electrodes, which presents a harmonic behavior directly related to the mass of the trapped ions. Through a Fourier transform of the recorded signal, it is therefore possible to measure the ions mass to charge ratio

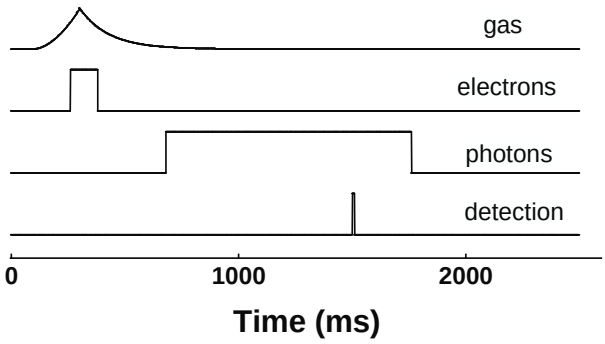

Figure 1: Schematic representation of a typical cycle used with the FT-ICR trap for the measurements at one photon energy. In this example, the target ions are first produced by 25 eV electron ionization of a gas pulse and, after a delay of 300 ms, further ionized during 1.1 second by synchrotron light pulse.

m/z, and their relative abundance. MICRA is a very simple and robust movable spectrometer, based on a 1.24 T permanent magnet, and has been specifically designed to allow a light beam to traverse the whole set-up [35]. The magnetic field allows for mass selection and detection in the *m/z* range from 4 to 500 u/q, with an ultimate resolving power of 73,000 at the mass of Xe^+ ion. The ICR cell is a cube with 2 cm sides. The two walls of the cell perpendicular to the photons propagation axis, used to excite the ions cloud, are replaced by an open structure to provide optical access without interference from surfaces. We estimate the number of trapped ions at a few hundred thousand and the volume of the ion cloud in the range of 0,05 cm^3 leading to an ion density in the middle of the trap to be of the order of 10^6 cm^{-3}. The nominal pressure in the cell is in the low 10^{-9} mbar. Figure 1 illustrates a typical time sequence produced for data acquisition at a given photon energy. The target ions are first produced by ionization of rare gas atoms in the gas pulse by 25 eV kinetic energy electrons. In this example, after a delay of Δt =300 ms, the ions are irradiated for 1100 ms by the monochromatized synchrotron radiation, and the mass spectrum of ions in the trap is then recorded. Chopping of the synchrotron radiation beam is performed using a pneumatic activated shutter. The mass spectrum measured at one photon energy is then obtained from the Fourier transform of the signal resulting from the average of 60 to 100 repetitive cycles, similar to the one presented on figure 1. It is important to note that, in the energy range considered here, neither the energy of the photons or the electrons alone is sufficient to produce doubly-charged ions from double ionization of the atoms (the thresholds are 38.36 eV and 33.10 eV for Kr and Xe atoms, respectively [30]). We have checked that no doubly-charged ions are produced when the photon pulse and/or the electron pulse are missing in the cycle. One useful characteristic of the FT-ICR ion trap is its ability to precisely select the ions stored inside the trap by increasing the kinetic energy of the unwanted ions until they hit the wall of the ICR cell. After irradiation the parent singly-charged ions were ejected to improve doubly-charged ion detection.
The best signal to noise ratio on the mass spectrum was obtained by performing the Fourier transform on the very beginning of the recorded signal, typically from 1.5 ms from the beginning to 3 ms. To obtain the photoionization spectra, the height of the doubly-charged signal in the mass spectrum was followed as a function of photon energy and corrected for the variation of the photon flux recorded using a gold mesh inserted at the exit of the photon beam line. For krypton, we used the height of the ^{84}Kr isotope line, and for xenon the mean of ^{129}Xe, ^{131}Xe and ^{132}Xe lines heights. The photon energy of the spectra was calibrated on the energy measured at ASTRID.

3. Results and discussion

3.1. Merged-beam experiment

The variation of the photoionization cross sections determined with the merged-beam set-up for Kr^+ and Xe^+ ions are shown on the upper- and lower-panel of figure 2, respectively. These spectra were obtained with a fixed width of the monochromator slit, resulting in a bandpass (BP) continuously increasing from 50 meV at threshold to 100 meV at 15 eV above threshold for the Kr^+ ion spectrum, and from 30 meV to 100 meV for the Xe^+ ion spectrum. The relative statistical uncertainties on the data at 30 eV photon energy are 6% and 16% for Kr^+ and Xe^+ ions, respectively. The cross section presented here for the Xe^+ ion is in good agreement with the one we have measured previously with lower resolution and statistics, using the same merged-beam set-up but a different ion source [21]. We note the close similarity of the Kr^+ and Xe^+ spectra in shape and intensity. Resonant structures are observed above the threshold and are followed by a smoothly decreasing continuum. Such similarity was already observed in the case of Br and I atoms, which are isoelectronic of Kr^+ and Xe^+ ions, respectively [36,37]. The integrated oscillator strengths of the spectra, calculated using [38]

$$f = 9.11\times10^{-3}\int \sigma(h\upsilon)dh\upsilon\,, \qquad (3)$$

are also of the same order, 1.40 and 1.49 for Kr^+ and Xe^+ ion, respectively .

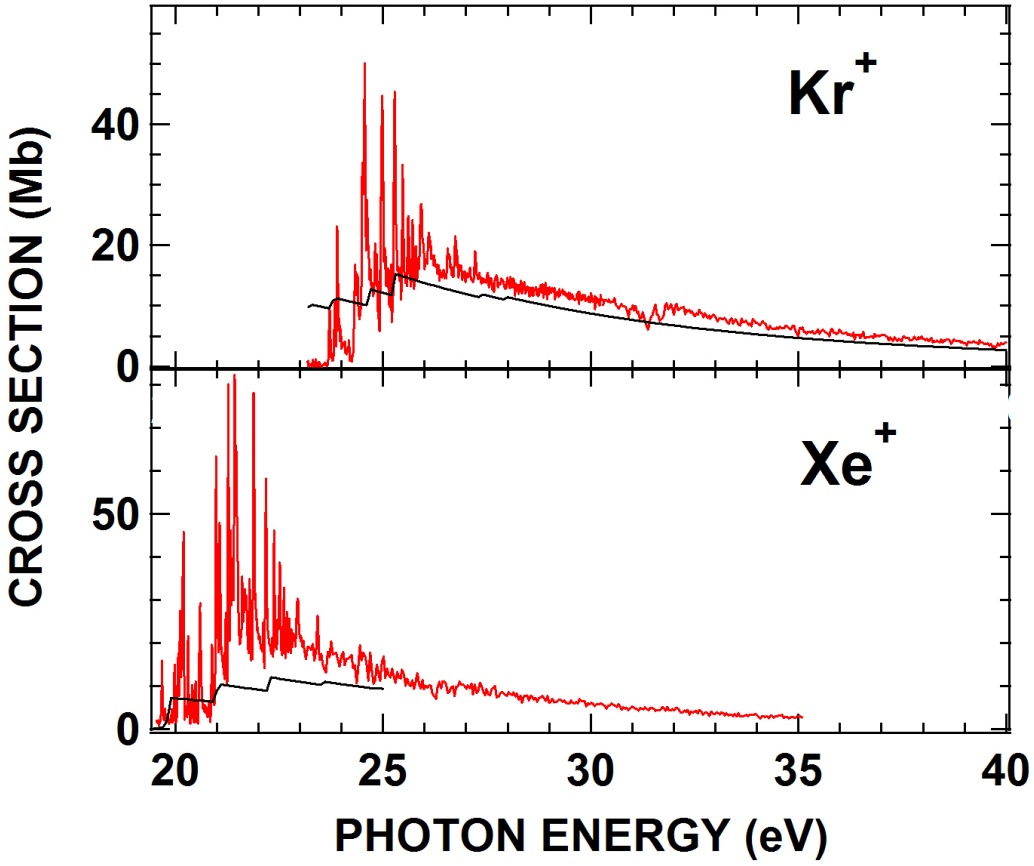

Figure 2: Variation as a function of the photon energy of photoionization cross sections measured with the merged-beam set-up for the Kr^+ ion (upper panel) and the Xe^+ ion (lower panel). The solid curves give the results of our MCDF calculations for the direct photoionization process.

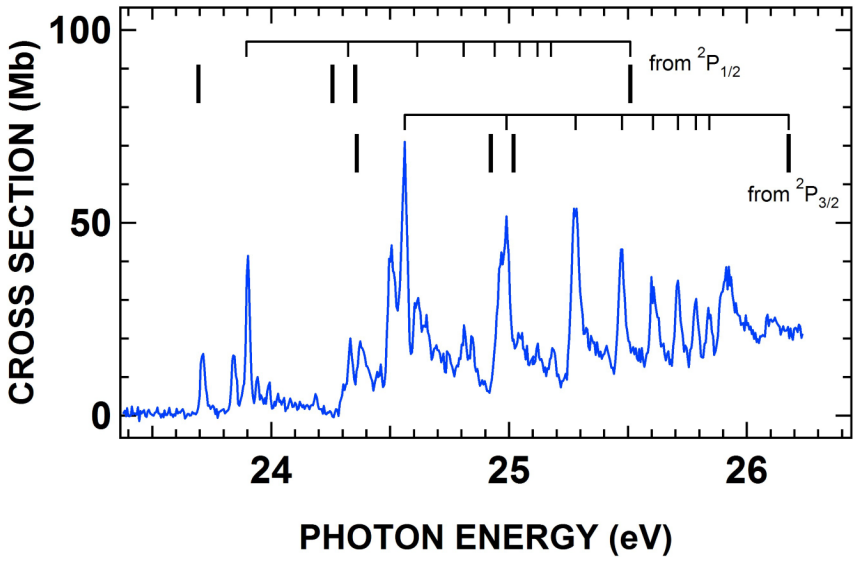

Figure 3: Enlargement of the photoionization cross section for Kr^+ ion close to thresholds recorded with an improved bandpass (mean value of 30 meV). The long vertical lines above the spectrum give the position of the np^4 (n = 4) ionization thresholds for the ions in the $np^5\ ^2P_{3/2}$ ground level and $np^5\ ^2P_{1/2}$ metastable level [30], and the short ones the position of the $np^4\ ^1D_2$ md Rydberg series (see text).

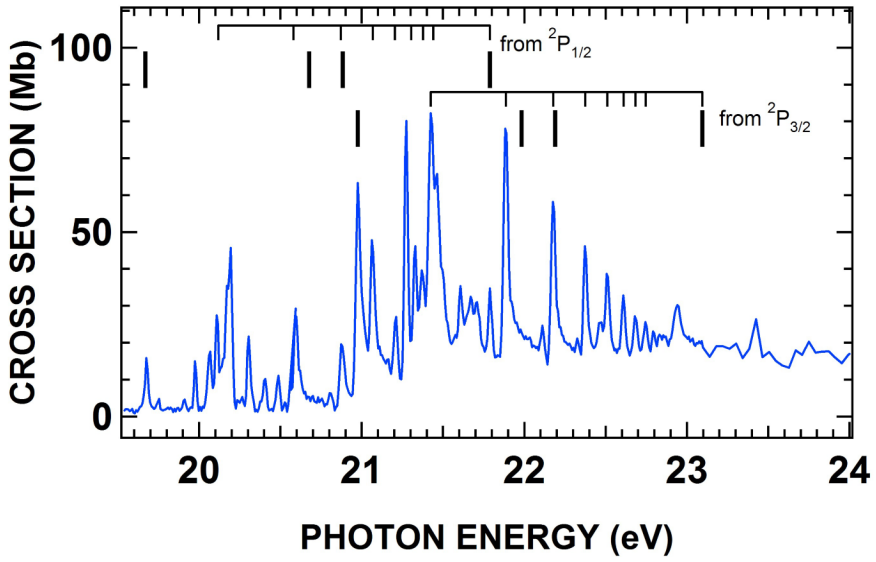

Figure 4: Same legend as figure 3 for Xe^+ ion (n=5) and a mean BP = 25 meV.

Enlargements of the resonance regions, obtained with an improved resolution compared to the spectra of figure 2, are shown on figure 3 for Kr^+ ion (BP = 20 to 40 meV) and figure 4 for Xe^+ ion (BP = 20 to 30 meV). The relative statistical uncertainties on these measurements are 7% and 4% for Kr^+ and Xe^+ ions, respectively. Kr^+ and Xe^+ ions are halogen-like with one hole in the p outer-subshell, giving an electronic configuration $np^5\ ^2P_{3/2}$ (n = 4 for Kr and n = 5 for Xe) in their ground level. The long vertical lines above the spectra indicate the position of the various $np^4\ ^3P_{2,1,0}$ and $^1D_2$ ionization thresholds (the $^1S_0$ threshold is at higher energy than covered by the figures) [30]. The first excited level $np^5\ ^2P_{1/2}$ is metastable, with lifetimes of 340 ms and 49 ms for Kr^+ and Xe^+ ions, respectively [39]. For both ions, the strong lines observed below the first ionization threshold of the ions in the ground level testify to the contribution of ions in the $^2P_{1/2}$ metastable level. These ions are produced inside the ion source and have enough time to travel to the interaction region, the time of flight needed for the transfer being a few µs. The np^4 ionization thresholds for the ions in the metastable level are also indicated on figures 3 and 4 [30].

The lines observed on the spectra can be attributed to excitation of the valence shell electron by electric-dipole allowed processes, giving rise to the transitions $np^5 \rightarrow np^4 ms, md$. The np^4 *ms,md* excited states decay via autoionization to the ground level of the doubly-charged ion. Rydberg states of *ms* and *md* character converging to each of the four upper np^4 levels are expected to be observed in photoionization spectra, giving rise to rich structures of intricate Rydberg series. The situation is even worse once we consider the important contribution of the ions in the metastable level, doubling the number of expected lines. For halogen atoms, only the very sophisticated eigenchannel *R*-matrix approach has been able to satisfactorily reproduce the experimental spectra, in particular the strongly asymmetrical profile of some Rydberg series resulting from an interference effect between the direct and the resonant photoionization processes [40]. Considering the moderate energy resolution chosen in this work to compensate for the low density of target ions, we have not attempted a detailed identification of the observed structures, which are most of the time composed of several unresolved lines. An analysis can be achieved using the formula:

$$E_n = E_\infty - \frac{RZ^2}{(n-\delta)^2} \qquad (4)$$

where R, E_∞ , Z and δ are the Rydberg constant, the converging limit, the electric charge of the core ion and the quantum defect, respectively. The ionization thresholds E_∞ were taken from [30] and we assumed Z = 2. The measured energy E_n, the quantum defect and the assignment resulting

from this analysis are given in tables 1 and 2 for Kr^+ and Xe^+ ions, respectively. For both ions, the dominant structures are associated with Rydberg series converging to the $^1D_2$ limit, with principal quantum number m going up to 13. The positions of the lines of these series are shown as the short vertical lines on figures 3 and 4, both for ions initially in the ground and the metastable terms. The relative intensities of the two series indicates a relative population of the two terms close to the statistical weight. For Kr^+ ion, series converging to the $^1S_0$ can also be identified and the quantum defect is almost constant along the series. The analysis is more difficult for Xe^+ ion, only the series converging to the $^1D_2$ limit being clearly identified but with a less constant quantum number along the series than for Kr^+ ion.

Table 1. Energy, quantum defect and assigment of the Rydberg series obtained using equation (4) for the Kr^+ ion.

Energy (eV)	δ	Assignment
23.712	0.02	$^2P_{1/2} \rightarrow ^3P_1$ 10d
23.845	0.29	$^2P_{1/2} \rightarrow ^1S_0$ 4d
23.902	0.18	$^2P_{1/2} \rightarrow ^1D_2$ 6d
24.334	0.20	$^2P_{1/2} \rightarrow ^1D_2$ 7d
24.501	0.29	$^2P_{3/2} \rightarrow ^1S_0$ 4d
24.562	0.19	$^2P_{3/2} \rightarrow ^1D_2$ 6d
24.613	0.21	$^2P_{1/2} \rightarrow ^1D_2$ 8d
24.811	0.17	$^2P_{1/2} \rightarrow ^1D_2$ 9d
24.989	0.23	$^2P_{3/2} \rightarrow ^1D_2$ 7d
		$^2P_{1/2} \rightarrow ^1D_2$ 10d
25.047	0.15	$^2P_{1/2} \rightarrow ^1D_2$ 11d
25.119	0.20	$^2P_{1/2} \rightarrow ^1D_2$ 12d
25.18	0.15	$^2P_{1/2} \rightarrow ^1D_2$ 13d
25.280	0.20	$^2P_{3/2} \rightarrow ^1D_2$ 8d
		$^2P_{1/2} \rightarrow ^1S_0$ 5d
25.475	0.19	$^2P_{3/2} \rightarrow ^1D_2$ 9d
25.605	0.23	$^2P_{3/2} \rightarrow ^1D_2$ 10d
25.710	0.19	$^2P_{3/2} \rightarrow ^1D_2$ 11d
25.785	0.19	$^2P_{3/2} \rightarrow ^1D_2$ 12d
25.842	0.23	$^2P_{3/2} \rightarrow ^1D_2$ 13d
25.91	0.38	$^2P_{3/2} \rightarrow ^1S_0$ 5d
26.10	0.33	$^2P_{1/2} \rightarrow ^1S_0$ 6d
26.58	0.31	$^2P_{1/2} \rightarrow ^1S_0$ 7d
26.74	0.38	$^2P_{3/2} \rightarrow ^1S_0$ 6d
27.23	0.35	$^2P_{3/2} \rightarrow ^1S_0$ 7d
27.53	0.38	$^2P_{3/2} \rightarrow ^1S_0$ 8d
31.38		$^2P_{3/2} \rightarrow 4s4p^5\ ^3P_2$ 5p

31.69	$^2P_{3/2} \rightarrow 4s4p^5\ ^3P_1\ 5p$
35.0	$^2P_{3/2} \rightarrow 4s4p^5\ ^3P\ 6p$

Table 2. Same as table 1 for the Xe^+ ion

Energy (eV)	δ	Assignment
20.195	0.16	$^2P_{1/2} \rightarrow {}^1D_2\ 6d$
20.594	0.25	$^2P_{1/2} \rightarrow {}^1D_2\ 7d$
20.876	0.28	$^2P_{1/2} \rightarrow {}^1D_2\ 8d$
21.062	0.34	$^2P_{1/2} \rightarrow {}^1D_2\ 9d$
21.210	0.30	$^2P_{1/2} \rightarrow {}^1D_2\ 10d$
21.425	0.29	$^2P_{3/2} \rightarrow {}^1D_2\ 6d$
21.886	0.29	$^2P_{3/2} \rightarrow {}^1D_2\ 7d$
22.177	0.30	$^2P_{3/2} \rightarrow {}^1D_2\ 8d$
22.375	0.31	$^2P_{3/2} \rightarrow {}^1D_2\ 9d$
22.510	0.35	$^2P_{3/2} \rightarrow {}^1D_2\ 10d$
22.610	0.41	$^2P_{3/2} \rightarrow {}^1D_2\ 11d$
22.683	0.51	$^2P_{3/2} \rightarrow {}^1D_2\ 12d$
22.747	0.49	$^2P_{3/2} \rightarrow {}^1D_2\ 13d$

At higher photon energy, the smoothly decreasing cross sections are due to the direct photoionization process

$$ns^2np^5\,^2P_{3/2,1/2} + h\nu \rightarrow ns^2np^4\,^3P_{2,1,0}\ ^1D_2\ ^1S_0 + e^- \quad (5)$$

We have performed multiconfiguration Dirac-Fock (MCDF) calculations using the code developed by Bruneau [41] to calculate the direct photoionization cross section. We considered all of the levels with an np^5 configuration in the initial state and np^4 in the final ionic state. For each initial state, the photoionization cross sections were calculated with a regular interval of the photon energy of 0.1 eV close to thresholds and 0.5 eV above. The result of these calculations for the Kr^+ ion is shown as the solid line on the top panel of figure 2. In the case of the Xe^+ ion (lower panel), the solid line is the result of our previously published calculations performed using the same code [21]. Both theoretical cross sections have been reconstructed assuming a statistical population of the ions in the $^2P_{3/2}$ ground level and $^2P_{1/2}$ metastable level. Let us note that, save at the opening of the various ionization thresholds, the magnitude of the reconstructed cross section is quite insensitive to the relative abundance of ions in the two levels. Our calculations show that the photoionization cross section is almost the same for the ions in the ground and the metastable levels, as can be expected from a monoconfigurational approach, demonstrating the weak effect of electron correlations for this process. For both ions, the calculations reproduce correctly the variation of the cross sections with photon energy, but with a magnitude 15 to 30% systematically lower than the measurements.

On the upper panel of figure 2, clear window resonances are observed at photon energy of 31.38 eV and 31.69 eV. They can be interpreted as the n = 5 term of the Kr^+ $4s4p^5$ ($^3P_{2,1}$) np Rydberg series which have a series limit at 38.73 eV and 39.16 eV [29]. Kr^+ $4s4p^5$ (^3P) 6p member could be associated with the weak structure at 35.0 eV. Kikas et al [42] propose 31.62 eV and 34.86 eV for the n = 5 and n = 6 members of the $4s\ 4p^5(^3P)\ np\ ^2S$ series, respectively.

3.2. FT-ICR ion trap

The spectra obtained for Kr^+ ion using the FT-ICR ion trap at different delay times Δt between the production of the ions and their irradiation by synchrotron radiation are displayed on the two lower panels of figure 5. They are compared with the spectrum recorded using the merged-beam set-up

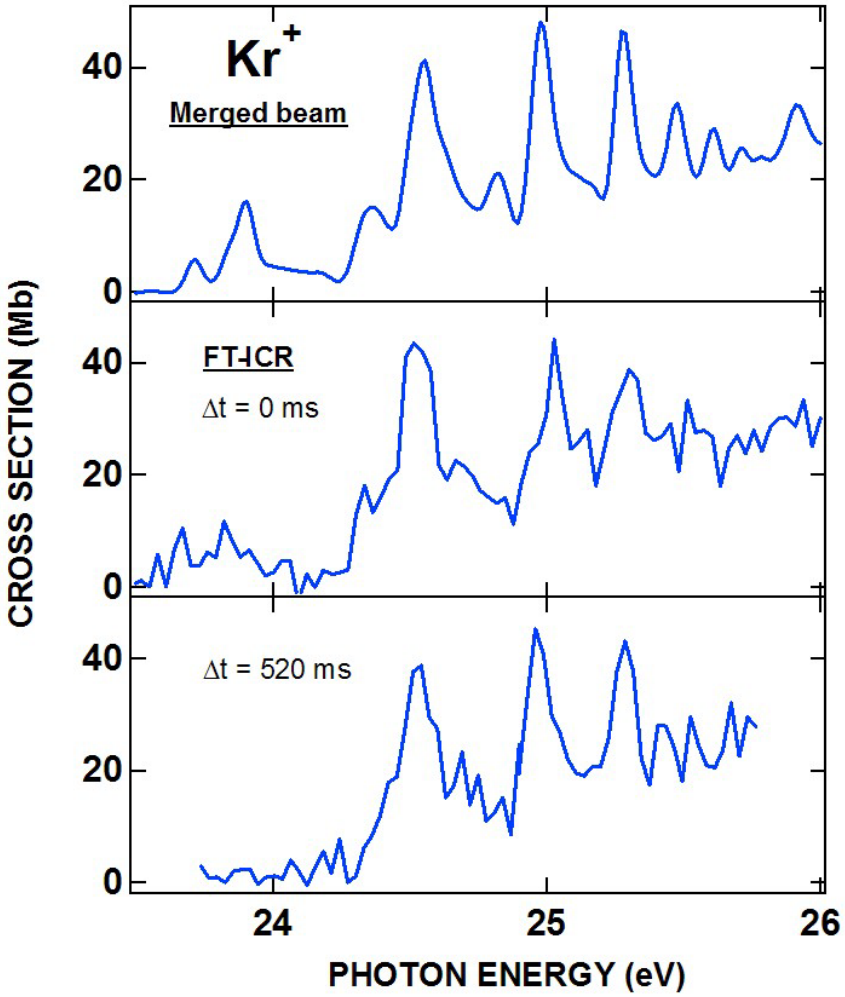

Figure 5: Comparison of the spectra obtained for the Kr^+ ion using the merged-beam set-up (upper panel) and the FT-ICR ion trap at two different delays between the production of the ions inside the trap and their irradiation by synchrotron radiation: Δt=0 (middle panel) and Δt=520ms (lower panel).

shown on the upper panel. It is the same spectrum than the one on figure 3, but convolved with a Gaussian profile to achieve the same apparent excitation bandpass (100 meV) and thus to make comparison between the spectra recorded with the two techniques easier. The spectra obtained with the ion trap are placed on an absolute scale assuming that the integrated area under the FT-ICR ion trap spectrum is identical to the merged-beam spectrum. The one on the middle panel was obtained by irradiating the Kr^+ ions just after their production inside the trap (Δt=0). Despite a larger statistical scatter, it displays the same structures as those seen on the merged-beam spectrum, demonstrating that the ions produced in the trap are both in the ground $^2P_{3/2}$ and in the metastable $^2P_{1/2}$ levels, and with abundances close to those observed in the merged-beam set-up. On the lower panel, the delay between production and irradiation was increased to Δt =520 ms, a longer time than the natural lifetime of the metastable level (350 ms) allowing most of the ions in this level to radiatively decay to the ground level. The intensity of the structures below the first

ionization threshold at 24.36 eV has been strongly reduced, demonstrating that the ions irradiated inside the trap now are mostly in the ground level.
The main loss of trapped ions often comes from charge exchange with the water molecules in the residual gas inside the trap. As the ionization potential of xenon atom is lower than water, charge exchange with water is inhibited and the trapping time of Xe^+ ions can be extended without major losses. Figure 6 shows the spectrum recorded at ELETTRA with the same trap with a delay of more than one second [21], corresponding to twenty times the natural lifetime of the $^2P_{1/2}$ meta-

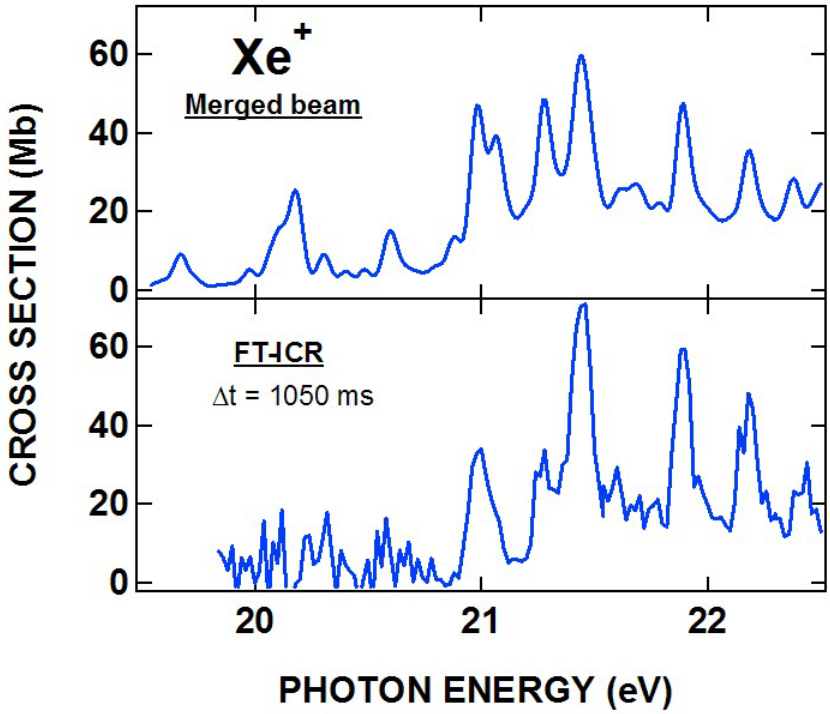

Figure 6: Comparison of the spectra obtained for the Xe^+ ion using the merged-beam set-up (upper panel) and the FT-ICR ion trap (lower panel).

stable level. It is compared to the spectrum of figure 4 convolved with a Gaussian profile to achieve the same overall resolution. As was the case previously, the ion trap spectrum was placed on an absolute scale by equating the integrated areas of the two spectra. Once again, the structures below the first ionization threshold (20.98 eV) are strongly reduced in intensity, thus demonstrating that most of the irradiated ions are in their ground level.
We observe no effect of the trapping magnetic field of 1.24 T on the position of the lines. The MCDF code has been used to quantify the magnetic field effect on both Xe^+ $5p^5$ and Xe^{2+} $5p^4$ levels. Each ionic charge state has been separately considered. For each M_J value, the energies of the sublevels have been calculated by diagonalization of the Hamiltonian matrix including contributions of the magnetic field interaction evaluated on the basis of unperturbed wave functions. The shift produced by a field of 1.24 T has a maximum amplitude of 0.15 meV for Xe^+ $5p^5$ and 0.21 meV for Xe^{2+} $5p^4$. Such values are well below the resolution of our experiments.

4. Conclusion

We have measured the photoionization cross sections of halogen-like Kr^+ and Xe^+ ions in an energy range extending up to 15 eV above the threshold. Two different set-ups were used, a merged-beam set-up at ASTRID and a FT-ICR ion trap at SOLEIL. The merged-beam set-up has

allowed the identification of the main resonant structures in the spectra, as well as the determination of the absolute cross sections for the direct photoionization process. Comparison of the photoionization spectra obtained using the trap and the merged-beam experiment has allowed extraction of the pure ground state ionization cross section on an absolute scale. MCDF calculations suitably reproduce the variation of the direct photoionization cross section.

This work demonstrates that the implementation of an ion trap experiment at a third generation synchrotron radiation beam line is a valuable tool that allows the measurement of the photoionization cross section of ionic species in their ground state if the lifetimes of metastable states are significantly shorter than the ion storage time. Photoionization experiments on stored ions are still difficult owing to (i) the very low density of target ions and (ii) the limitation in trapping time resulting from charge exchange and reactions with the residual gas. Nevertheless, there is no doubt that such experiments will be developed in the future, as demonstrated by the recent results obtained on multiply-charged ions [25] and ionic clusters [26]. Concerning the coupling of a permanent magnet FT-ICR trap with synchrotron radiation, improvements can be obtained by increasing the number of stored ionic species and by achieving a better overlap between the ion cloud and the photon beam. Such a device is under development with a cylindrical permanent magnet producing in its centre a magnetic field coaxial with the axis of the cylinder. The cell will also be larger than in the MICRA instrument. In this way ions can be produced externally to the magnetic field region and then be transferred inside the trap. Since all high pressure events are in a separate chamber the analyzer cell is operated with improved vacuum. This is useful for investigations over a wide wavelength range. Radio-Frequency traps are also very promising instruments for the study of mass selected ions as demonstrated recently at SOLEIL [43], but they operate with a helium buffer gas which restricts their use to photon energies smaller than 24.5 eV, the helium ionisation threshold.

The high resolution of the FT-ICR mass spectrometer (MS) and its MS/MS capability make it a powerful tool for the study of photoionization processes on molecular ions. Up to now, only two experiments have been published, both on the CO^+ ion using merged-beam set-ups [44,45]. Such studies with merged-beam set-ups have not been further developed, partly due to the strong background which can be observed in the photoionization spectra. We will use the MICRA trap to study photoionization processes on small molecular ions, in particular of interest in planetology.

Acknowledgements

The authors would like to thank the support of the European Community – Research Infrastructure Action under FP6 Structuring the European Research programme (IA-SFS, contract number RII3-CT-2004-506008). They are also grateful to the ISA staff of the Aarhus University and to the staff of SOLEIL and, in particular, of the DESIRS beam line for their helpful assistance. One of us (ARM) acknowledges the support by the Ministry of Science and Technological Development of Republic of Serbia under Project No. 141011.

References:

[1] Riccardo V, Andrew P, Ingesson L C and Maddaluno G 2002 *Plasma Phys. Contr. Fusion* **44** 905
[2] Bakhtiari M, Kawano Y, Tamai H, Miura Y, Yoshino R and Nishida Y 2002 *Nucl. Fusion* **42** 1197
[3] Federici G *et al* 2001 *Nucl. Fusion* **41** 1967
[4] ITER Physics Basis 1999 *Nucl. Fusion* **39** 2137
[5] Carroll P K and Costello J 1986 *Phys. Rev. Lett.* **57** 1581
[6] West JB 2001 *J. Phys. B* **34** R45
[7] Kjeldsen H 2006 *J. Phys. B* **39** R325
[8] Southworth et al 2007 *Phys. Rev. A* **76** 043421

[9] Sano M, Itoh Y, Koizumi T, Kojima T M, Kravis S D, Oura M, Sekioka T, Watanabe N, Awaya Y and Koike F 1996 *J. Phys. B: At. Mol. Opt. Phys.* **29** 5305
[10] Koizumi T *et al* 1997 *Phys. Scr.* T **73** 131
[11] Andersen P, Andersen T, Folkmann F, Ivanov V K, Kjeldsen H and West J B 2001 *J. Phys. B: At. Mol. Opt. Phys.* **34** 2009
[12] Itoh Y, Ito A, Kitajima M, Koizumi T, Kojima T M, Sakai H, Sano M and Watanabe N 2001 *J. Phys. B: At. Mol. Opt. Phys.* **34** 3493
[13] Gottwald A, Gerth C and Richter M 1999 *Phys. Rev. Lett.* **82** 2068
[14] Costello J T, Kennedy E T, Mosnier J P, Sayyad M H and McGuinness C 1998 *J. Phys. B: At. Mol. Opt. Phys.* **31** L547
[15] Kjeldsen H, Kristensen B, Brooks R L, Folkmann F, Knudsen H and Andersen T 2002 *Astrophys. J. Suppl.* **138** 219
[16] Covington A M *et al* 2001 *Phys. Rev. Lett.* **87** 243002
[17] Aguilar A *et al* 2003 *Astrophys. J. Suppl.* **146** 467
[18] Kjeldsen H, Folkmann F, Innocenti F, Zuin L and Hansen J E 2002 *J. Phys. B: At. Mol. Opt. Phys.* **35** L375
[19] Schippers S *et al* 2002 *Phys. Rev. Lett.* **89** 193002
[20] Schippers S *et al* 2003 *Nucl. Instrum. Methods Phys. Res. B* **205** 297
[21[Thissen R, Bizau J M, Blancard C, Coreno M, Dehon C, Franceschi P, Giuliani A, Lemaire J and Nicolas C 2008 *Phys Rev Lett* **100** 223001
[22] Kravis SD *et al* 1991 *Phys Rev Lett* **66** 2956
[23] Kravis SD *et al* 1992 *Phys. Rev. A* **45** 6379
[24] Epp SW *et al* 2007 *Phys. Rev. Lett.* **98** 183001
[25] Simon M C *et al* 2010 *J. Phys. B: At. Mol. Opt. Phys.* **43** 065003
[26] Hirsch K, Lau J T, Klar P, Langenberg A, Probst J, Rittmann J, Vogel M, Zamudio-Bayer V, Möller T and von Issendorff B 2009 *J. Phys. B: At. Mol. Opt. Phys.* **42** 154029
[27] Kjeldsen H, Folkmann F, van Elp J, Knudsen H, West J B and Andersen T 2005 *Nucl. Instrum. Methods Phys. Res. B* **234** 349
[28] Miyake K P, Kato R and Yamashita H 1969 *Sci. Light* **18** 39
[29] Samson J A R 1967 *Techniques of Vacuum Ultra Violet Spectroscopy*, John Wiley & Sons, New York
[30] Ralchenko Yu, Kramida A E, Reader J and NIST ASD Team 2010. *NIST Atomic Spectra Database* (ver. 4.0.0), [Online]. Available: http://physics.nist.gov/asd [2010, September 30]. National Institute of Standards and Technology, Gaithersburg, MD.
[31] Almen O and Nielsen K 1957 *Nucl. Instr. and Meth.* **1** 302
[32] Rinn K, Müller A, Eichenauer H and Salzborn E 1982 *Rev. Sci. Instrum.* **53** 829
[33] Lemaire J *et al* 2002 *Phys. Rev. Lett.* **89** 273002
[34] Dunbar C, Polfer N C and Oosmens J 2007 *J. Am. Chem. Soc.* **129** 14562
[35] Mauclaire G, Lemaire J, Boissel P, Bellec G and Heninger M 2004 *Eur. J. Mass Spectrom.* **10** 155
[36] Ruscic B, Greene J P and Berkowitz J 1984 *J. Phys. B: At. Mol. Phys.* **17** 1503
[37] Berkowitz J, Batson C H and Goodman G L 1981 *Phys. Rev. A* **24** 149
[38] Fano U and Cooper J W 1968 *Rev. Mod. Phys.* **40** 441
[39] Jullien S, Lemaire J, Fenistein M, Mauclaire G and Marx R 1993 *Chem. Phys. Lett.* **212** 340
[40] Robicheaux F and Greene C H 1992 *Phys. Rev. A* **46** 3821
[41] Bruneau J 1984 *J. Phys. B: At. Mol. Phys.* **17** 3009
[42] Kikas A, Osborne S J, Ausmees A, Svensson S, Sairanen O P and Aksela S 1996 *J. Electron Spectrosc. Relat. Phenom.* **77** 241
[43] Giuliani A, Milosavljević A R, Scuderi D, Lemaire J, Dehon D, Thissen R, Nicolas C, Refregiers M, Maitre P and Nahon L, Private Communication
[44] Andersen T, Kjeldsen H, Knudsen H and Folkmann F 2001 *J. Phys. B* **34** L327
[45] Hinojosa G et al 2002 *Phys. Rev. A* **66** 032718